# Quench Behavior of Prototype Nb-Ti HL-LHC Dipole Canted Cos-Theta Orbit Corrector Magnets

Mariusz Wozniak, Emmanuele Ravaioli, Franco Mangiarotti, Matthias Mentink, Glyn Kirby, Arjan Verweij, Qingjin Xu, and Wei Wu

***Abstract*—The HL-LHC project is an upgrade of the LHC that requires double aperture dipole correctors. In 2015, CERN selected Canted Cos-Theta (CCT) magnet, and the development of the MCBRD magnets followed. Since then, a prototype (P1) has been built and measured at CERN, and quench results agree with simulations. In 2017, China joined the programme with in-kind prototypes and twelve (four spares) series magnets with WST, IMP, IHEP, and BAMA efforts. The first MCBRD magnet built in China is the second prototype (P2) of the programme. This magnet was subjected to triggered energy extractions at CERN magnet test facility. The energy extraction is used for magnet protection, keeping voltage-to-ground and hot-spot temperature below 560 V and 250 K, respectively. A high magnetic-field change rate during the magnet discharge from high currents causes a substantial quench-back due to the heat generated by the eddy currents in the magnet formers. A specialized software, ProteCCT, was developed as part of the STEAM project to simulate such a unique quench behaviour. This contribution focuses on comparing measured results between the P1 and P2 magnets, and P2 quench measurement and simulation results. The correction factors available in the ProteCCT software allow matching the measured results. We identify measurements needed to refine simulation inputs further and improve the simulation predictive capability.**

***Index Terms*—Canted cosine theta (CCT), HL-LHC, quench simulation, superconducting magnet protection.**

## I. Introduction

THE HL-LHC upgrade requires eight 105 mm warm bore diameter, double aperture dipole correctors on both sides of ATLAS and CMS, each with a horizontal and a vertical field [1]. In 2015, CERN selected a Canted Cos-Theta (CCT) magnet design, and the development of the MCBRD magnets followed. The CCT technology development at CERN involved a range of experiment and simulation activities. A short prototype was built and tested [2]. The specialized simulation tool, ProteCCT [3], [4], was developed as part of the STEAM project [5]. Later on, the first full-length double aperture prototype, MRBRDP1 (referred below as P1), was built and measured at CERN [6]. The quench simulation results calculated with the ProteCCT software were consistent with those measurements [7].

In 2017, China joined the programme with an in-kind contribution of prototypes and twelve (four spares) series magnets with Western Superconducting Technologies Co. Ltd. (WST), Institute of High Energy Physics (IHEP), Institute of Modern Physics (IMP), both of the Chinese Academy of Sciences (CAS), and Suzhou Bama Superconductive Technology Co. Ltd. (BAMA) efforts. Work progresses in the frame of CERN's collaboration with IHEP. WST built the first prototype of the collaboration, the MRBRDP2 presented here (referred below as P2). The magnet was trained to an ultimate current of 422 A at 4.0 K at the IMP. The P2 magnet was transported to CERN and subjected to a series of forced energy extractions at a range of currents, extraction resistances, and at 1.9 K. The reported measurements of the P1 and the P2 magnets were performed at the CERN superconducting magnet test facility.

A comparison between the P1 and P2 magnets is made in terms of built differences and measurement results. The ProteCCT software was used for the simulation of the energy extraction transients of both magnets. It turns out that for the P2 magnet, a different set of correction factors is needed, and we present and discuss the correction factors providing the best fit to the measurements. We identify additional measurements needed to refine simulation inputs further and improve the simulation predictive capability of the ProteCCT software. Finally, based on the P2 results, we conclude if the HL-LHC project protection baseline for MCBRD 1.4 Ω [1] is adequate to respect the limits on voltage-to-ground and coil hot-spot temperature of 560 V [8] and 250 K [9], respectively.

## II. MCBRD Magnet

The MCBRD magnet features two helically wound tilted concentric coils per aperture, wound on aluminium alloy formers with an opposite inclination. The coils cancel each other's solenoid magnetic field component and superpose the dipole components [10]–[12]. The magnet is 2.2 m long and, at a nominal current of 394 A, generates a peak magnetic field of 2.94 T at the windings. The magnet is wound with round, 825 $\mu$m bare diameter, Nb-Ti/Cu superconducting (SC) composite wire with 82 $\mu$m thick polyimide tape wrap insulation. The formers provide a mechanical structure for the windings and play a role during a quench. An outer cylinder provides mechanical

Manuscript received November 25, 2021; revised February 17, 2022 and March 14, 2022; accepted March 31, 2022. Date of publication April 13, 2022; date of current version May 2, 2022. *(Corresponding author: Mariusz Wozniak.)*

Mariusz Wozniak, Emmanuele Ravaioli, Franco Mangiarotti, Matthias Mentink, Glyn Kirby, and Arjan Verweij are with CERN, 1211 Meyrin, Switzerland.

Qingjin Xu is with the Institute of High Energy Physics, Chinese Academy of Sciences, Beijing 100000, China.

Wei Wu is with the Institute of Modern Physics, Chinese Academy of Sciences, Lanzhou 730000, China.

Color versions of one or more figures in this article are available at https://doi.org/10.1109/TASC.2022.3167341.

Digital Object Identifier 10.1109/TASC.2022.3167341

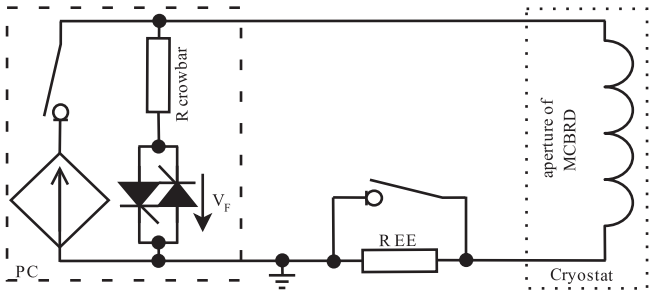


Fig. 1. Schematic of magnet powering during tests. Abbreviations: PC – power converter, EE – energy extraction, and $V_F$ – forward voltage.

TABLE I
KEY DIFFERENCES BETWEEN MCBRD PROTOTYPE MAGNETS

| Part | Characteristic | MCBRDP1 | MCBRDP2 | Unit |
|---|---|---|---|---|
| Formers | RRR | 8 | 4.14 | - |
| | fLoopFactor* | 2 | 0.8 | - |
| Wire | Cu:SC | 1.95:1 | 1.18:1 | - |
| | Ic, 7 T, 4.2 K | 660 | 776 | A |
| | Cu RRR | 230 | 184 | - |
| Test circuit** | R crowbar | 50 | 7 | mΩ |

*Simulations parameter described in the text and listed here for clarity.
**Measurement circuit parameter listed here for clarity.

protection and support of the outer former. The formers and cylinder are made of a 6082 T6 aluminium alloy. The cold iron yoke serves as a return path for the magnetic field.

## III. POWERING AND PROTECTION

Each magnet aperture was powered independently during tests according to the circuit schematic in Fig. 1. The quench detection settings do not affect the forced energy extraction results presented here. The power converter (PC) is switched off, and the energy-extraction (EE) switches are opened to initiate the forced energy extraction. In fact, the output stage of the PC's DC/DC converter changes to a high impedance and the magnet current is commuted to the PC's internal crowbar resistor (Table I) and thyristors, with the forward voltage $V_F$ of 1 V. The forced energy extractions on the P2 magnet were performed in individual tests with the EE resistance of 2.0 Ω for each apertures and 1.4 Ω for the aperture 2 only.

## IV. MEASUREMENT OF SIMULATION INPUTS

Measurements in this section apply to the P2 magnet only.

### A. Formers RRR

Three 4 x 6 x 100 $mm^3$ cuboids of the former material were machined and characterized with a 4-wire electrical resistance measurement, with voltage taps spaced 50 mm apart and a DC current of 1 A, passing in both directions [13]. The measured resistivity was 46.9 nΩ m at 273 K and 11.3 nΩ m at 4.2 K, resulting in a RRR of 4.14 (listed in Table I).

### B. Wire Cu RRR

During the cooldown of the P2 magnet at CERN, a 4-wire measurement of the coils was performed at 293 K and 10 K using magnet voltage taps [14]. The weighted average of the measured RRR of the various coil sections was 180. The wire Cu RRR was calculated to be 184, based on the wire Cu:SC ratio and assuming the Nb-Ti RRR of 1.155.

### C. Magnet Inductance

The measured inductance of each aperture was 0.97 H and constant in a range of 100–300 A [14]. Above, due to the iron-yoke saturation, the inductance monotonically decreased to 0.94 H at 422 A. In the ProteCCT simulations, we used an inductance of 0.505 $Hm^{-1}$, calculated from the inductance at low current divided by the magnetic length of 1.92 m.

## V. SIMULATIONS

ProteCCT software [4] (the same version as in [7]) was used for simulating the magnet behaviour during a discharge. ProteCCT software is free-to-use and part of the STEAM project [5]. It is a lumped-element tool for simulating discharge transients in CCT superconducting magnets with conductive formers. The calculation method considers fully three-dimensional quench behaviour using a simplified representation of the CCT coil geometry. Thermal propagation along the length of the strands as well as transverse to the formers is considered. More software details are available in the ProteCCT manual [3] and in the publication comparing measurement and simulation results for the P1 magnet [7]. There are two global correction factors available in ProteCCT. The fLoopLength is a factor by which the formers resistivity is multiplied to account for the effective path length of the currents flowing in the formers and outer cylinder. The addedHeCpFrac corresponds to a fraction of the former volume that is occupied by the helium. This adds helium heat capacity to the heat capacity of the formers.

The simulated circuit corresponds to the measurements circuit. However, the voltage drop $V_F$ over the thyristors in series with the crowbar was neglected. The $V_F$ is about 1 V, and hence only a small fraction of the extraction voltage. The impact on the simulations results is therefore considered negligible.

## VI. COMPARISON OF P1 AND P2 MAGNETS

### A. Magnet Components

The P1 and P2 magnets are different, and the key differences are listed in Table I. The 6082 alloy RRR used in simulations of the P1 magnet was 8, and the fLoopFactor was adjusted to a value of 2 to obtain the best match between simulations and experimental results [7]. WST manufactured in China the P2 magnet wire. The lower Cu:SC ratio of the P2 magnet wire as compared to the P1 magnet wire results in P2 wire with 21% and 53% higher resistance per meter at 273 K and 10 K, respectively.

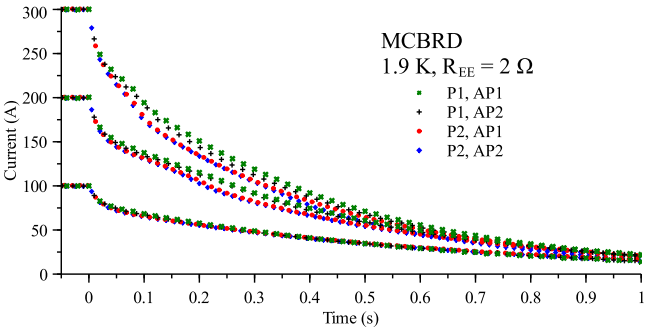


Fig. 2. Comparison of measured current decays at various currents and between apertures of the P1 and the P2 magnets. All for forced energy extractions at time of 0 s and with 2 Ω EE resistance and at 1.9 K.

### *B. Results of Forced Energy Extractions*

The P1 and P2 prototypes have been extensively measured at various currents, temperatures and EE resistances. However, it is only at 1.9 K and 2 Ω EE where both prototypes have been measured, and the current versus time curves are plotted in Fig. 2. A direct comparison between the magnets is complicated due to small differences in the powering circuits (see Table I [7], [14], [15]). Depending on the initial extraction current, distinctive current decay features are noticeable. For discharges from 300 A, a quench-back occurs in both prototypes. A longer time constant of the P1 discharge could be attributed to the lower wire resistance per meter. For discharges from 200 A, the quench back occurs in the P2 magnet, with a characteristic "kink" at about 0.2 s, but not in the P1 magnet. This behaviour could not be attributed to a difference in the current sharing temperature, $T_{CS}$, suggesting the P1 magnet winding starts generating heat at a lower temperature. At 200 A and 1.49 T, the $T_{CS}$ are 7.86 K and 8.06 K for the P1 and P2 magnet wires, respectively. It should be noted that the resins used for winding impregnation of the P1 and P2 magnets are different, and we can speculate that the resin used for the P2 magnet has different thermal conductivity and/or specific heat. As a result, in the P2 magnet, the heat generated in the formers is more effective in causing the windings to quench. For discharges from 100 A, there is no quench-back, and the magnet inductance and the EE and crowbar resistances dominate the discharge. In addition, there are contributions of inductances and resistances from the metal structures, mainly the formers. Those metal parts contribute in a similar way as a shorted secondary winding of a transformer. With the available test data, we cannot conclude which of the contributions mentioned above dominates the difference in the discharges from 100 A.

## VII. Measurements and Simulations for the P2 Magnet

A comparison of measured and simulated currents and voltages for aperture 2 of the P2 magnet and 1.4 Ω EE resistance is shown in Figs. 3(a) and 4, respectively, and for currents in Fig. 3(b) for the 2 Ω EE resistance. The voltage-to-ground limit of −560 V is plotted with the red dashed line in Fig. 4, and the used protection scheme is compliant with it. A good degree

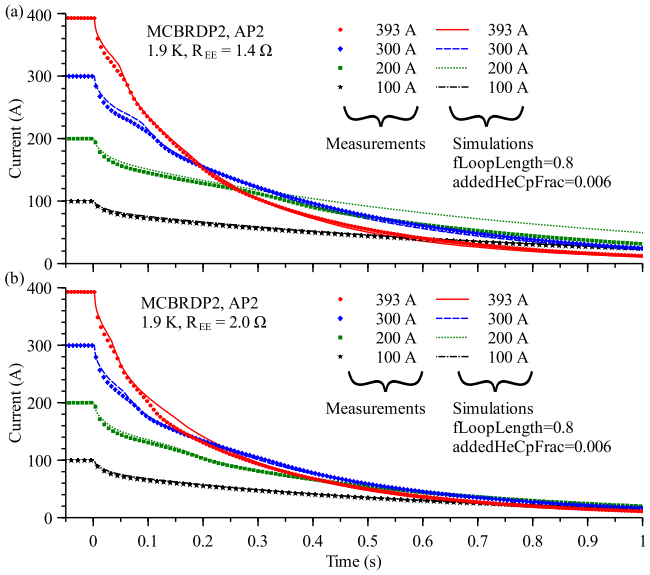


Fig. 3. Measured and simulated current decays for aperture 2 of the P2 magnet at 1.9 K and with EE resistance of (a) 1.4 Ω, (b) 2 Ω.

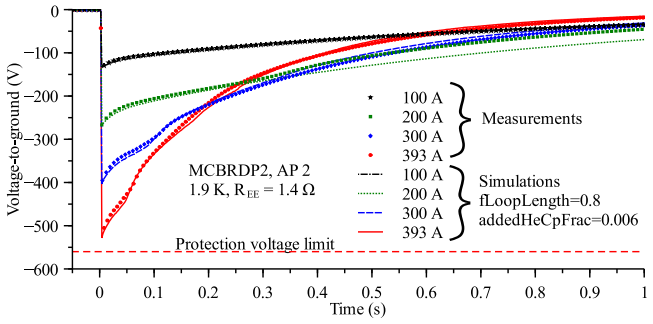


Fig. 4. Measured and simulated voltages to ground for aperture 2 of the P2 magnet at 1.9 K and with EE resistance of 1.4 Ω (HL-LHC project baseline).

of consistency between simulation results and experimental observations was achieved by the appropriate choice of the two global correction factors available in ProteCCT [3]. The addedHeCpFrac was set to 0.006, i.e., the same as for the P1 magnet [7]. The fLoopLength was adjusted predominantly due to the different RRR of the formers used in simulations of the P2 magnet, see Table I. A value of 0.8 was chosen based on the best fit between measured and simulated discharge integrals (integral of $I^2dt$) in high current regions, as illustrated in Fig. 5. There are two characteristic steps in the simulated current discharge integrals, see Fig. 5(a). The first occurs around 200 A for the 1.4 Ω EE resistance and divides regions with and without the quench-back. The step is affected by the EE resistance and is at around 175 A for 2 Ω. The step is affected by fLoopLength, and a good fit to the measured 200 A extraction is for fLoopLength of 0.6. This value, however, results in a discrepancy for the higher values of the initial extraction current. The current level of the step of the discharge integral is also affected by the addedHeCpFrac, as plotted in Fig. 6 for the fLoopLength of 0.8. However, even adjusting the addedHeCpFrac to 0 does

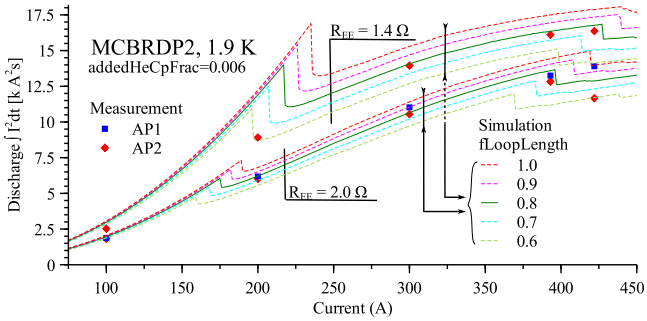


Fig. 5. Measured and simulated discharge integrals for the P2 magnet at 1.9 K and with EE resistance and apertures: (a) 1.4 Ω and aperture 2, (b) 2 Ω and both apertures.

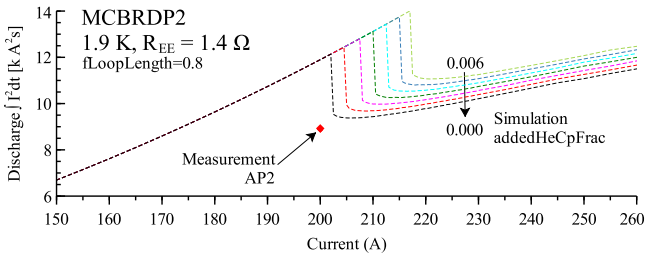


Fig. 6. Comparison of measured and simulated discharge current integrals for aperture 2 of the P2 magnet at 1.9 K and with EE resistance of 1.4 Ω.

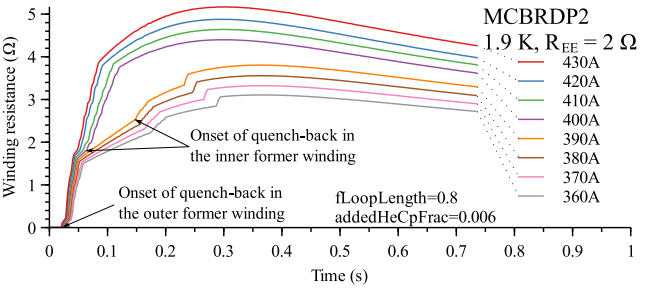


Fig. 7. Simulated winding resistance evolution in time for a range of the initial extraction currents for the P2 magnet and with 2 Ω EE resistance and at 1.9 K.

not match the measured 200 A discharge integral. The second step change of the simulated discharge integral occurs at about 400 A for the 2.0 Ω EE resistance. This step could be explained by a plot of the magnet winding's resistance versus time for a range of extraction currents, as shown in Fig. 7. A distinct change in resistance evolution in time is visible between the initial current of 390 A and 400 A. It is due to the different times of quench-back in the inner former winding, as indicated by arrows in Fig. 7. The inner former has enhanced cooling due to direct contact with helium and as a result its winding quench-back later.

## VIII. Discussion

Fig. 8 shows the adiabatic hot-spot temperature as a function of the discharge current integral assuming a constant field of 3.25 T (for the ultimate current). As in [7], we have assumed 3.6 kA$^2$

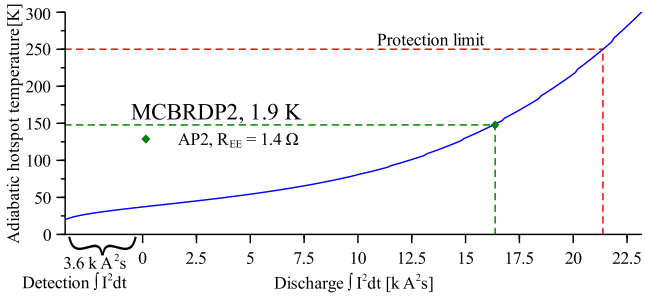


Fig. 8. Calculated at 3.25 T adiabatic hotspot temperature for the P2 magnet wire vs discharge current integral. The measured point corresponds to the highest discharge current integral in Fig. 4(a). The protection temperature limit is shown with red dashed lines.

s for the detection, as marked on the horizontal axis. The point plotted corresponds to the highest discharge integral measured at the ultimate current of 422 A and the HL-LHC baseline EE resistance of 1.4 Ω [1]. The adiabatic hot-spot temperature is about 150 K and well below the limit of 250 K [9], marked by the red dashed line.

During forced energy extractions, the formers absorb magnet stored energy and substantially affect the quench behaviour of the magnet. The measured resistivity of 46.9 nΩ m at 273 K, as given in Section IV A, is rather high for the 6082 T6 alloy, as compared to a value of 36 nΩ m at 273 K, estimated from 38 nΩ m at 293 K reported by several manufacturers (for example [16]). On the other hand, used internally in the ProteCCT scaling of the 6082 T6 aluminium alloy resistivity results in values of 35.1 nΩ m and 30.18 nΩ m at 273 K for RRR of 4.14 and 8 (the latter used in simulations of P1 in [7]), respectively. Without going into a detailed discussion of the impact of the combination of the uncertainty of RRR and the room temperature resistivity on the 1.9–9.2 K temperature range, critical for quench simulations, we can conclude that measured and used internally in ProteCCT resistivity values need further refinement. After such corrections and rerunning quench models, one could comment on potential differences in the fLoopLength of 0.8 reported here for the P2 and 2 used in [7] for the P1 simulations. A new measurement of resistivity of 6082 T6 used for the P1 and P2 magnets is in progress at CERN. The step changes in the simulated discharge integrals provide an interesting opportunity to validate further the assumptions made in the ProteCCT tool and its inputs and correction parameters. Additional data could be obtained from a measurement campaign with forced energy extractions where the initial extraction current is adjusted in response to changes of the measured current integrals to best capture or rule out a potential step. More measured discharge integrals would support a more sophisticated refinement of the fLoopLength and addedHeCpFrac. The simulations would have to combine both factors that correctly match the value of the current discharge integral and the position of the step regarding the initial discharge current. We also note here that the resins used in the P1 and P2 magnets are different. The thermal conductivity and heat capacity data, if available, could be used in the ProteCCT software.

## IX. Summary

The measured responses of MCBRDP1 and MCBRDP2 to the forced energy extractions are different, and we described and discussed their key characteristics. A good degree of consistency between simulation results and experimental observations is demonstrated for a range of initial currents and energy extraction resistances for the MCBRDP2 magnet. However, adjusting the correction factors fLoopLength and addedHeCpFrac, available in the ProteCCT software, was needed to correct for resistance and eddy current path length and the helium fraction that might have penetrated the windings. A need for further refinement of simulation inputs and a more strategic measurement of the energy extraction integrals was identified. Based on the results, we conclude that the HL-LHC project protection baseline of 1.4 Ω EE resistance for the MCBRD magnet is still adequate for protection with the defined limits for the hot-spot temperature and voltage-to-ground.

## References


[1] E. Todesco *et al.*, "High-Luminosity Large Hadron Collider (HL-LHC): Technical design report. Insertion magnets," *CERN Yellow Rep., Monographs*, vol. 10, 2020, doi: 10.23731/CYRM-2020-0010.

[2] F. J. Mangiarotti *et al.*, "Test of short model and prototype of the HL-LHC D2 orbit corrector based on CCT technology," *IEEE Trans. Appl. Supercond.*, vol. 29, no. 5, Aug. 2019, Art. no. 4002305, doi: 10.1109/TASC.2019.2897347.

[3] M. Mentink, "STEAM-ProteCCT user manual," *CERN EDMS 2160020*, 2019. [Online]. Available: https://edms.cern.ch/document/2160020

[4] M. Mentink, J. v. Nugteren, F. Mangiarotti, M. Duda, and G. Kirby, "Quench behavior of the HL-LHC twin aperture orbit correctors," *IEEE Trans. Appl. Supercond.*, vol. 28, no. 3, Apr. 2018, Art. no. 4004806, doi: 10.1109/TASC.2018.2794451.

[5] STEAM Project Website. [Online]. Available: https://espace.cern.ch/steam

[6] F. J. Mangiarotti *et al.*, "Test of the first full-length prototype of the HL-LHC D2 orbit corrector based on Canted Cosine Theta technology," *IEEE Trans. Appl. Supercond.*, vol. 30, no. 4, Jun. 2020, Art. no. 4000505, doi: 10.1109/TASC.2020.2969637.

[7] M. Mentink, M. Duda, F. Mangiarotti, J. v. Nugteren, G. Willering, and G. Kirby, "Simulated versus experimentally observed quench behavior of the HL-LHC twin aperture orbit corrector prototype," *IEEE Trans. Appl. Supercond.*, vol. 30, no. 4, Jun. 2020, Art. no. 4701306, doi: 10.1109/TASC.2020.2970389.

[8] T. D. C. R. da Rosa *et al.*, "Electrical design criteria for the HL-LHC D2 orbit corrector," *CERN EDMS* 2363906, 2021. [Online, restricted access]. Available: https://edms.cern.ch/document/2363906/1.0

[9] M. Mentink *et al.*, "Quench protection of the HL-LHC RCBRD circuits," *CERN EDMS* 2222746, 2019. [Online, restricted access]. Available: https://edms.cern.ch/document/2222746/1

[10] J. Rysti and E. Todesco, "Conceptual design of the orbit correctors for D2 and Q4," Geneva, Switzerland, Rep. No. ACC-2015-0060, 2015. [Online]. Available: http://cds.cern.ch/record/2026461

[11] G. A. Kirby *et al.*, "Hi-Lumi LHC twin-aperture orbit correctors magnet system optimization," *IEEE Trans. Appl. Supercond.*, vol. 27, no. 4, Jun. 2017, Art. no. 4002805, doi: 10.1109/TASC.2016.2633424.

[12] G. A. Kirby *et al.*, "Hi-Lumi LHC twin aperture orbit correctors 0.5 m model magnet development and cold test," *IEEE Trans. Appl. Supercond.*, vol. 28, no. 3, Apr. 2018, Art. no. 4002205, doi: 10.1109/TASC.2017.2782683.

[13] F. O. Pincot, "RRR measurement of CCT former in IHEP -after heat treatment," *CERN EDMS* 2381976 v.1, 2020. [Online, restricted access]. Available: https://edms.cern.ch/document/2381976/1

[14] F. J. Mangiarotti *et al.*, "Test summary of MCBRDP2," *CERN EDMS* 2436078 v.1.0, 2021. [Online, restricted access]. Available: https://edms.cern.ch/document/2436078/1

[15] F. J. Mangiarotti *et al.*, "Test summary of MCBRDP1," *CERN EDMS* 2046092 v.1.1, 2019. [Online, restricted access]. Available: https://edms.cern.ch/document/2046092/1.1

[16] Allco website, "Aluminium alloy 6082 - T6 datasheet," Accessed: Nov. 2021. [Online]. Available: https://www.aalco.co.uk/datasheets